Dalton Transactions

ROYAL SOCIETY OF CHEMISTRY

PAPER

View Article Online
View Journal | View Issue

Cite this: *Dalton Trans.*, 2021, **50**, 12495

$[(V^{IV}O)_2M^{II}_5]$ (M = Ni, Co) Anderson wheels†

Hector W. L. Fraser, ‡[a] Emily H. Payne, ‡[a] Arup Sarkar, [b] Lucinda R. B. Wilson,[a] Dmitri Mitcov,[c] Gary S. Nichol, [a] Gopalan Rajaraman, *[b] Stergios Piligkos *[c] and Euan K. Brechin *[a]

Received 26th May 2021,
Accepted 2nd July 2021

DOI: 10.1039/d1dt01710a

rsc.li/dalton

Heterometallic Anderson wheels of formula $[(V^{IV}O)_2M^{II}_5(hmp)_{10}Cl_2](ClO_4)_2{\cdot}2MeOH$ (M = Ni, **1**; Co, **2**) have been synthesised from the solvothermal reaction of $M(ClO_4)_2{\cdot}6H_2O$ and VCl_3 with hmpH (2-(hydroxymethyl)pyridine). The metallic skeleton describes a centred hexagon, with the two vanadyl ions sitting on opposing sides of the outer ring. Magnetic susceptibility and magnetisation measurements indicate the presence of both ferromagnetic and antiferromagnetic exchange interactions. Theoretical calculations based on density functional methods reproduce both the sign and strength of the exchange interactions found experimentally, and rationalise the parameters extracted.

Introduction

Alongside its prominent role in polyoxometalate chemistry,[1] vanadium has had significant impact in the field of molecule-based magnetism. For example, orthogonal magnetic orbitals were exploited to produce ferromagnetic exchange in a $[(V^{IV}O)$–$Cu^{II}]$ dimer,[2] the Prussian blue $V[Cr(CN)_6]_{0.86}$ was one of the initial examples of a coordination compound exhibiting room temperature magnetic order,[3] single-molecule magnet behaviour was observed in a $[V^{III}_4]$ butterfly,[4] $[V_{30}]$ and $[V_{15}]$ have been widely studied to examine the influence of geometrical spin-frustration and antisymmetric exchange,[5] and most recently monometalic V^{IV} compounds such as $(Bu_4N)_2[V(C_8S_8)_3]$ and [VOPc] have been touted as excellent candidates for electron-spin based qubits.[6]

Heterometallic 3d cages containing vanadium are however rather rare, and indeed those containing nickel or cobalt are relatively scarce. A search of the Cambridge Structural Database reveals only eight (Ni) and sixteen (Co) unique structure types with a nuclearity of four or more. When the nuclearity is increased to seven or more metal ions this number reduces to just four (Ni) and five (Co) examples.[7] Restricting the search to complexes of any nuclearity containing the V^{IV}–O–M^{II} (M = Ni, Co) moiety, and excluding polyoxometalates,[8] surprisingly affords only two different structure types: [(VO)M] dimers,[9] and a single $[(VO)_6M]$ wheel.[10] The latter complex has the formula $[MV^{IV}_6O_6\{(OCH_2CH_2)_2N(CH_2CH_2OH)\}_6]X$ (X = halide) in which the six vanadyl moieties form a wheel that 'encapsulates' a variety of s- and 3d metal ions (M).[10] Given the paucity of such species we have begun a program of research aimed at synthesising a variety of heterometallic $V^{IV}O$-3d cluster compounds. The recent success we have had in employing the ligand 2-(hydroxymethyl)pyridine (hmpH) in the construction of heterometallic Anderson wheels of general formula $[M^{III}_2M^{II}_5(hmp)_{12}]^{4+}$ (where M^{III} = Cr, Al and M^{II} = Mn, Fe, Co, Ni, Cu, Zn),[11] hinted that this might be a viable route to isolating similar M^{IV}–M^{II} cages.

Experimental

Experimental procedures

All chemicals were procured from commercial suppliers and used as received (reagent grade). **Caution:** although no issues were encountered here care should be taken when handling potentially explosive perchlorate salts.

Synthesis of $[(VO)_2Ni_5(hmp)_{10}Cl_2](ClO_4)_2{\cdot}2MeOH$ (1)

$Ni(ClO_4)_2{\cdot}6H_2O$ (0.366 g, 1 mmol) and VCl_3 (0.079 g, 0.5 mmol) were dissolved in MeOH (24 ml) with NaOMe (0.162 g, 3 mmol) to give a green solution. Upon full dissolution, hmpH (0.285 ml, 3 mmol) was added dropwise resulting in a darkening of the solution colour. The reaction was left overnight with continuous stirring. 10 ml samples of the resulting dark green solution

[a]*EaStCHEM School of Chemistry, The University of Edinburgh, David Brewster Road, Edinburgh, EH9 3FJ Scotland, UK. E-mail: E.Brechin@ed.ac.uk*
[b]*Department of Chemistry, Indian Institute of Technology Bombay, Powai, Mumbai 400076, India. E-mail: rajaraman@chem.iitb.ac.in*
[c]*Department of Chemistry, University of Copenhagen, Universitetsparken 5, 2100 Copenhagen, Denmark. E-mail: piligkos@chem.ku.dk*

†Electronic supplementary information (ESI) available: Additional crystallographic, magnetic and theoretical data. CCDC 1847956 and 1847957. For ESI and crystallographic data in CIF or other electronic format see DOI: 10.1039/d1dt01710a

‡These authors contributed equally.

were heated in Teflon-lined autoclaves at 140 °C for 24 hours. After slowly cooling to room temperature the reaction vessels were allowed to sit undisturbed for 24 hours yielding dark green, triangular prism-shaped crystals suitable for X-ray diffraction. Yield 0.126 g (34.2% by Ni weight). Anal. Calcd (%) for $C_{62}H_{68}Cl_4N_{10}Ni_5O_{22}V_2$: C 40.42, H 3.72, N 7.60, Ni 15.93, V 5.53; found: C 40.24, H 3.42, N 7.34, Ni 16.00, V 5.75.

Synthesis of $[(VO)_2Co_5(hmp)_{10}Cl_2](ClO_4)_2\cdot 2MeOH$ (2)

$Co(ClO_4)_2\cdot 6H_2O$ (0.366 g, 1 mmol) and VCl_3 (0.079 g, 0.5 mmol) were dissolved in MeOH (24 ml) with NaOMe (0.162 g, 3 mmol) to give a red/orange solution. Upon full dissolution, hmpH (0.285 ml, 3 mmol) was added dropwise resulting in a darkening of the solution colour. The reaction was left overnight with continuous stirring. 12 ml samples of the resulting solution were heated in Teflon-lined autoclaves at 100 °C for 12 hours. After slowly cooling to room temperature the reaction vessels were allowed to sit undisturbed for 24 hours yielding red, plate-shaped single crystals suitable for X-ray diffraction. Yield 0.130 g (35.3% by Co weight). Anal. Calcd (%) for $C_{62}H_{68}Cl_4N_{10}Co_5O_{22}V_2$: C 40.39, H 3.72, N 7.58, Co 15.98, V 5.53; found: C 40.02, H 3.51, N 7.56, Co 16.11, V 5.76.

Crystallographic details

Diffraction data for compound **1–2** were collected using a Rigaku Oxford Diffraction SuperNova diffractometer with MoK_α radiation (Table 1). An Oxford Cryosystems Cryostream 700+ low temperature device was used to maintain a crystal temperature of 120 K. The structures were solved using ShelXT and refined with ShelXL interfaced through Olex2.[12,13] All non-hydrogen atoms were refined using anisotropic displacement parameters. H atoms were placed in calculated positions geometrically and refined using the riding model. CCDC: 1847956 and 1847957.† Powder XRD measurements were performed using a Bruker D2 PHASER spectrometer, and are shown in Fig. S1.†

Table 1 Crystallographic information for compounds **1–2**

Compound	**1**	**2**
Formula	$C_{62}H_{68}Cl_4N_{10}Ni_5O_{22}V_2$	$C_{62}H_{68}Cl_4Co_5N_{10}O_{22}V_2$
$D_{calc.}$/g cm^{-3}	1.721	1.712
μ/mm^{-1}	1.779	1.613
Formula weight	1842.49	1843.59
Colour	Dark green	Pale brown
Shape	Block	Plate
Size/mm^3	0.52 × 0.29 × 0.16	0.50 × 0.14 × 0.06
T/K	120.0	120.0
Crystal system	Monoclinic	Monoclinic
Space group	$P2_1/n$	$P2_1/n$
a/Å	15.7800(3)	15.7439(9)
b/Å	12.4392(2)	12.4867(5)
c/Å	19.0165(4)	18.9773(12)
α/°	90	90
β/°	107.745(2)	106.591(6)
γ/°	90	90
V/Å^3	3555.16(12)	3575.4(4)
Z (Z')	2 (0.5)	2 (0.5)
Wavelength/Å	0.71073	0.71073
Radiation type	MoK_α	MoK_α
Θ_{min}/°–Θ_{max}/°	3.072–32.985	3.079–28.897
Measured refl.	90 810	37 370
Independent refl.	12 777	8344
Reflections used	10 678	5589
R_{int}	0.0447	0.0715
Parameters	516	479
Restraints	155	1
Largest peak	0.678	1.013
Deepest hole	−0.475	−0.678
GooF	1.042	1.041
wR_2 (all data) (wR_2)	0.0770 (0.0719)	0.1612 (0.1465)
R_1 (all data) (R_1)	0.0461 (0.0341)	0.1147 (0.0704)

Magnetisation data collection

Magnetic susceptibility and magnetisation measurements in the temperature range T = 2–290 K were performed on a Quantum Design MPMS XL SQUID magnetometer equipped with a 5 T dc magnet in the field range, B = 0.1–5.0 T. Samples were mounted in gelatine capsules and restrained by addition of a small quantity of hexadecane. The observed paramagnetic susceptibilities were corrected for diamagnetic contributions using Pascal's constants.

Computational details

Density functional theory (DFT) calculations were carried out using Gaussian 09 (Rev D.01).[14] The unrestricted hybrid B3LYP functional along with the all-electron triple-ζ valence (TZV) basis set was used to evaluate the spin state energies for all atomic centres, performed on crystal structures. SCF convergence criteria were set to tight using the quadratic convergence method, followed by a stability test as implemented in G09. Overlap integral calculations were carried out to reveal the extent of magnetic exchange occurring between neighbouring metal centres. Local magnetic anisotropies on the Co^{II} ions were computed using *ab initio* methods in ORCA 4.0.1.[15] During these local zero-field splitting (zfs) calculations, paramagnetic metal ions were substituted by diamagnetic Zn^{II} ions. Since the estimation of zfs and other spin-Hamiltonian (SH) parameters requires an accurate description of electronic excited states, the multi-configurational CASSCF-NEVPT2 method was applied. The scalar relativistic DKH Hamiltonian and DKH contracted version of basis sets (DKH-def2-TZVP for Co; DKH-def2-TZVP(-f) for Zn, N, O; DKH-def2-SVP for C, H) were used throughout the calculations. Spin–orbit coupling (SOC) and subsequent spin-Hamiltonian parameters were determined using the QDPT-EHA approach.[16] For Co(II), CAS(7,5) with ten quartets and forty doublets were allowed to mix in the SOC step.

Results and discussion

The reaction of $M(ClO_4)_2\cdot 6H_2O$ with VCl_3 and hmpH in a basic MeOH solution under solvothermal conditions produces crystals of $[(VO)_2M_5(hmp)_{10}Cl_2](ClO_4)_2\cdot 2MeOH$ (M = Ni, **1**; Co, **2**) in approximately 35% yield. Complexes **1–2** crystallise in the monoclinic space group $P2_1/n$ (Table 1) with half the cationic cage, one perchlorate counter ion and one molecule of methanol in the asymmetric unit. The metallic skeleton (Fig. 1)

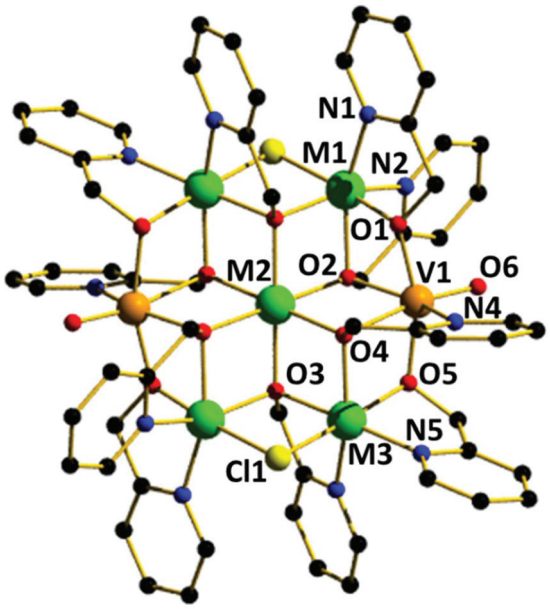

Fig. 1 Molecular structure of the cation in **1** and **2**. Colour code: V^{IV} = orange, M^{II} = green, Cl = yellow, O = red, N = blue and C = black. H-atoms, perchlorate counter ions and solvent molecules of crystallisation are omitted for clarity.

describes a centred $[(V^{IV}O)_2M^{II}_5]$ wheel in which the vanadyl moieties (V1 and symmetry equivalent, s.e.) oppose each other on the outer $[V^{IV}_2M^{II}_4]$ rim, *i.e.* they occupy positions 1, 4 (Fig. 4). The central M^{II} ion (M2, position 7, Fig. 4) is bridged to the six outer ring metals by six μ_3-OR groups from six deprotonated hmp ligands. The four remaining hmp ligands each provide a μ-OR bridge on the exterior of the ring between one V^{IV} ion and one M^{II} ion. The two opposing Cl ions also μ-bridge in the external wheel, between M1 and M3 (positions 2 and 6, respectively, Fig. 4) and s.e. All seven metal ions display distorted octahedral coordination geometries, with the vanadyl moiety having a V=O bond length of ~1.6 Å (Tables S1 and 2†).

The perchlorate anions and MeOH molecules of crystallisation H-bond to each other (O···O, ~2.8 Å), sitting in-between the planes of the cationic cages (Fig. S2†). The closest intermolecular contacts between cations exist between aromatic rings on neighbouring molecules with C(Ar)···H(Ar) separations in the range ~2.3–2.8 Å, and between the aromatic rings and the Cl ions, (Ar)···Cl at ~2.9 Å.

In the extended structure the cations pack in columns down the *b* axis, with the columns arranged into rows with each neighbouring column composed of molecules which are eclipsed with respect to the adjacent column (Fig. S3†).

Complexes **1**–**2** are structurally related to the $[M^{III}_2M^{II}_5(hmp)_{12}]^{4+}$ (M^{III} = Cr, Al and M^{II} = Mn, Fe, Co, Ni, Cu, Zn) family of Anderson wheels,[11] the species $[MV^{IV}_6O_6\{(OCH_2CH_2)_2N(CH_2CH_2OH)\}_6]^{n+}$ (M = Li, Na, Mg, Mn, Fe, Co, Ni) reported by Khan,[10] and the complex $[M^{II}_6Cr(HL_{zw})_6(HL)_6]^{3+}$ (M = Ni, Co; HL = 2-hydroxy-4-methyl-6-phenylpyridine-3-amidoxime) published by Murrie and Milios.[17] This highlights the apparent stability of the Anderson wheel structure, and the modular nature of the molecule whereby different metals in different oxidation states can be combined with the same (or similar) ligand sets to afford analogous species.[18] Note that in the $[M^{III}_2M^{II}_5(hmp)_{12}]^{4+}$ family, the M^{III} ion is positionally disordered around the external wheel. In $[M^{IV}_2M^{II}_5(hmp)_{10}]^{2+}$ (**1**–**2**) the M^{IV} is not positionally disordered.

Magnetic properties

The direct-current molar magnetic susceptibility, χ, of polycrystalline samples of complexes **1** and **2** were measured in an applied magnetic field, *B*, of 0.1 T, over the 2–290 K temperature, *T*, range. The experimental results are shown in Fig. 2 and 3 as the χT product *versus T*, where $\chi = M/B$ and *M* is the magnetisation.

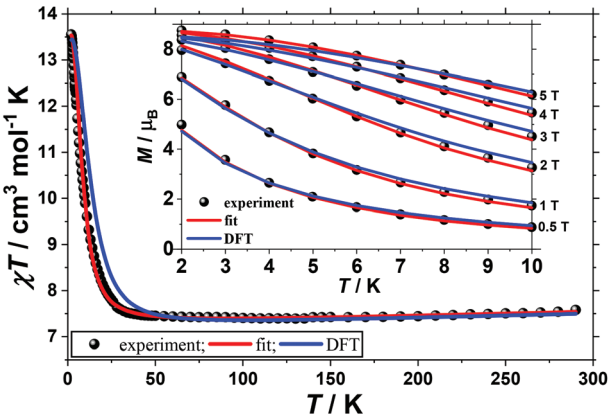

Fig. 2 Plot of the χT product *versus T* for **1** in an applied field, B = 0.1 T. Inset: Plot of the magnetisation (M) *versus* temperature (T) for **1** in the indicated field and temperature ranges. The red/blue lines are a fit of the experimental data as described in the text.

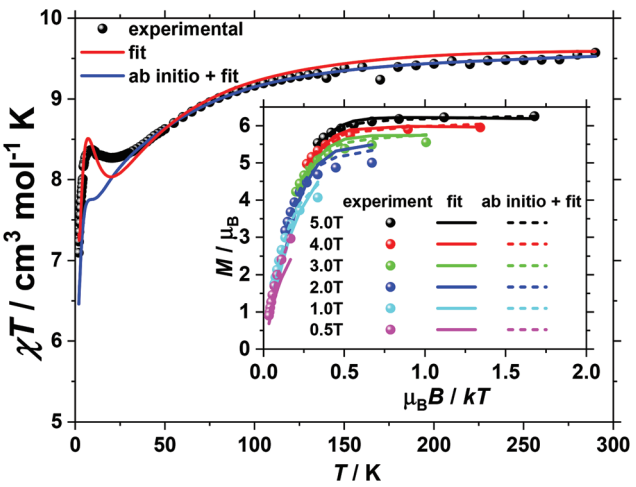

Fig. 3 Plot of the χT product *versus T* for **2** in an applied field, B = 0.1 T. Inset: Plot of the magnetisation *versus* field data for **2**. The solid and dashed lines are fits of the experimental and *ab initio* data, as described in the text.

At room temperature the χT product of **1** is 7.5 cm^3 K mol^{-1}, from where a g-value of g_{Ni} = 2.32 can be inferred based on the sum of Curie constants of five uncorrelated Ni^{II} ions (S_{Ni} = 1) and two uncorrelated V^{IV} ions (S_V = 1/2), with g_V = 2.00. Upon cooling the value of the χT product of **1** first slowly drops to reach 7.4 cm^3 K mol^{-1} at 100 K, then it slowly increases to reach 7.6 cm^3 K mol^{-1} at 30 K and finally rapidly increases below 30 K to reach 13.6 cm^3 K mol^{-1} at 2 K. This behaviour is indicative of competing antiferromagnetic and ferromagnetic interactions. To better define the low-temperature magnetic properties of **1**, variable-temperature-variable-field (VTVB) magnetisation measurements were performed in the temperature and field ranges 2 to 10 K and 0.5 to 5 T, respectively (inset of Fig. 2). The VTVB magnetisation of **1** at 2 K and 5 T reaches a maximum of 8.7μ_B (μ_B is the Bohr magneton). Notably, when the VTVB magnetisation data of **1** are plotted against the reduced quantity $\mu_B B/kT$ (k is the Boltzmann constant) no nesting of the VTVB curves is observed (Fig. S4†), indicative of negligible magnetic anisotropy.

For **2**, magnetisation measurements were performed on wet polycrystalline samples (of known mass, solvent content) because measurements performed on dry, powdered samples evidenced deterioration over time, consistent with PXRD data (Fig. S1†). This is likely due to lattice solvent loss, exacerbated by the reduced pressure conditions experienced by the sample during the SQUID measurements. The room temperature value of the χT product of **2** (Fig. 3) is 9.6 cm^3 K mol^{-1}, somewhat lower than the value of 10.125 cm^3 K mol^{-1} expected for five uncorrelated Co^{II} ions and two uncorrelated V^{IV} ions, assuming (*vide infra*) both that g = 2 for all centres (to avoid over-parameterisation) and that a low symmetry ligand field quenches the orbital angular momentum of the octahedral Co^{II} ions (*i.e.* spin-only S_{Co} = 3/2). Upon cooling the χT product of **2** drops continuously reaching a plateau value of 8.3 cm^3 K mol^{-1} at 20 K, whereupon it slightly increases to a local maximum of 8.5 cm^3 K mol^{-1} at 9 K, after which it drops to reach 7.1 cm^3 K mol^{-1} at 2 K. In contrast to **1**, when the VTVB magnetisation data of **2** are plotted against the reduced quantity $\mu_B B/kT$, significant nesting of the VTVB curves is observed (inset of Fig. 3), indicative of significant anisotropy.

The quantitative interpretation of the magnetic properties of **1** and **2** were performed by numerically fitting the experimental data to the full spin-Hamiltonian matrix, of dimension 972 for **1** and 4096 for **2**, by use of the simplex algorithm[19] and spin-Hamiltonian (1):

$$\hat{H} = \sum_i \left\{ \mu_B B g_i \hat{S}_i + D_i \left[\hat{S}_{i,z}{}^2 - \frac{S_i(S_i+1)}{3} \right] \right\} - 2 \sum_{i,j<i} J_{ij} \hat{S}_i \hat{S}_j \quad (1)$$

where the indices refer to the constituent metal ions, $\hat{S}$ is a spin operator, D_i is the single-ion uniaxial second order magnetic anisotropy parameter and J_{ij} is the pairwise isotropic exchange interaction. For simplicity, we assume all magnetic exchange interactions between M^{II}–M^{II} ions (J_{M-M}) and V^{IV}–M^{II} (J_{VO-M}) ions to be equivalent (Fig. 4, left). For **1**, given that the magnetic anisotropy is small, we fitted the temperature dependence of the χT product by neglecting the anisotropy terms in spin-Hamiltonian (1). This resulted in the best-fit parameters J_{Ni-Ni} = +1.30 cm^{-1} and J_{Ni-VO} = −3.49 cm^{-1}. Under these conditions the ground spin-state of **1** is an S = 4 state separated by about 6.2 cm^{-1} from the first excited state which is an S = 3 state (Fig. S5†). The magnetic anisotropy of the Ni^{II} ion was subsequently determined by fitting the VTVB data to spin-Hamiltonian (1) by varying the value of D_{Ni}, whilst keeping the J values fixed. This resulted in $|D_{Ni}|$ = 0.66 cm^{-1}.

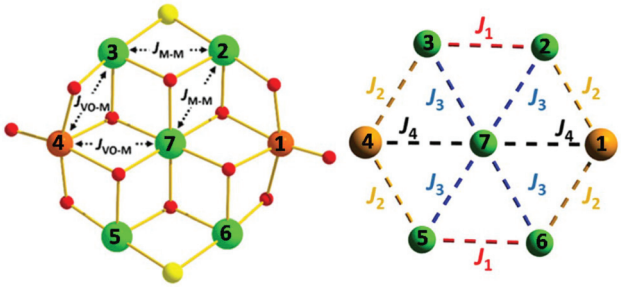

Fig. 4 (Left) Representation of the isotropic exchange interactions included in spin-Hamiltonian (1) used in the experimental fit of the susceptibility and magnetisation data for complexes **1** and **2**. (Right) The exchange interaction scheme used in the theoretical modelling of the magnetic data. Colour code as Fig. 1.

For **2**, the temperature dependence of the χT product was fitted to the full spin-Hamiltonian (1) resulting in the best fit parameters: J_{Co-Co} = −0.45 cm^{-1}, J_{Co-VO} = −4.85 cm^{-1} and $|D_{Co}|$ = 6.65 cm^{-1}. However, these parameters do not accurately reproduce the VTVB data (Fig. S6†). In order to obtain a better estimate of D_{Co}, the VTVB data of **2** were therefore fitted to spin-Hamiltonian (1) by fixing the values of the isotropic exchange and letting D_{Co} vary. This resulted in the best-fit parameter $|D_{Co}|$ = 21.40 cm^{-1}, with the resulting VTVB curves shown in the inset of Fig. 3. The persistent deviation of the calculated curves from the experimental data, originating from the simplicity of the model employed and assumptions made, therefore only allows us at this stage to estimate that $|D_{Co}|$ likely lies in the range 5 to 25 cm^{-1}.

The sign and magnitude of the exchange interactions in **1** and **2** are consistent with previous examples reported in the literature for both dialkoxo- and alkoxo/chloro-bridged M^{II}_2 units, and alkoxo-bridged (VO)–M^{II} moieties with similar bridging angles.[9,20–22]

Theoretical calculations

In order to further probe the magnitude and origin of the exchange interactions, and anisotropy of the Co^{II} ions, we now turn to theoretical methods. For this purpose we no longer assume that all magnetic exchange interactions between M^{II}–M^{II} ions (J_{M-M}) and V^{IV}–M^{II} (J_{VO-M}) ions are equivalent, but assign individual pairwise exchange interactions between the

constitutive centres in **1** and **2** (Fig. 4, right). Pairwise exchange interactions between neighbouring paramagnetic centres have been computed using the broken symmetry approach (Scheme S1,† eqn (S1)).[23] Four different isotropic exchange pathways (J_1–J_4) have been considered: $J_1 = J_{23} = J_{56}$ ($M^{II}_{(ring)}$–(Cl)(O)–$M^{II}_{(ring)}$); $J_2 = J_{12} = J_{34} = J_{45} = J_{16}$ ($M^{II}_{(ring)}$–(O)(O)–$V^{IV}_{(ring)}$); $J_3 = J_{27} = J_{37} = J_{57} = J_{67}$ ($M^{II}_{(ring)}$–(O)(O)–$M^{II}_{(centre)}$); $J_4 = J_{17} = J_{47}$ ($M^{II}_{(centre)}$–(O)(O)–$V^{IV}_{(ring)}$).

For **1**, the computed J values are shown in Table 2, together with the values obtained from numerical fitting of the experimental data for comparison. Calculation of the temperature dependence of the χT product and of the VTVB data using the DFT computed J values and neglecting the uniaxial anisotropy parameter for all metal centres results in good agreement with the experimental data (Fig. 2), with deviations mainly arising for the lower temperatures as a consequence of the isotropic model. The DFT computed J values suggest that the J_2 ($M^{II}_{(ring)}$–(O)(O)–$V^{IV}_{(ring)}$) interaction is relatively strongly antiferromagnetic, with all other interactions being weakly ferromagnetic in nature. This results in an $S = 4$ ground state, with the spin of the two V ions being antiparallel to the spins of the five Ni ions (Fig. S5†). The computed spin densities for the high spin state, as well as four broken symmetry (bs) solutions, provide values in the range of 1.66–1.74 for the Ni^{II} centres, and a spin polarized value of 1.12(1) for the VO centres (Fig. 5, S7, Table S3†). These are in good agreement with previously reported six coordinate Ni^{II} and V^{IV} species.[24] The reduced spin density values on the Ni ions indicate strong spin delocalisation onto the coordinating O, N and Cl ligand orbitals. The increased spin density value on the VO moiety reflects strong spin polarisation.

The computed isotropic exchange interactions for complex **1** can be rationalised by analysing the overlap of magnetic orbitals between interacting pairs of metal centres (Table S4 and Fig. S8†), together with their corresponding bridging angles (Table S1†). In the case of J_1 ($M^{II}_{(ring)}$–(Cl)(O)–$M^{II}_{(ring)}$), the Ni–Cl–Ni and Ni–O–Ni angles (84.2° and 103.2°, respectively) would be expected to result in a weak ferromagnetic interaction. For J_2 ($M^{II}_{(ring)}$–(O)(O)–$V^{IV}_{(ring)}$) the alkoxide bridging angles (Ni–O–V) are 104.27° (102.11°) and 96.81° (95.93°) and lead to significant antiferromagnetic coupling. Computation reveals significant overlap ($S_{Ni–V} = 0.07$) between the d_{xy} orbital of V^{IV} and the $d_{x^2-y^2}/d_{xz}$ orbitals of Ni^{II} – the lower symmetry and strong spin polarisation of the bridging oxygen atom maximises the V(d_{xy})–Ni($d_{x^2-y^2}/d_{xz}$) orbital overlap. J_3 ($M^{II}_{(ring)}$–(O)(O)–$M^{II}_{(centre)}$) is weakly ferromagnetic in nature, due to the presence of small Ni–O–Ni angles (96°–100°).[25,26] J_4 is also weakly ferromagnetic because of minimal overlap between magnetic orbitals.

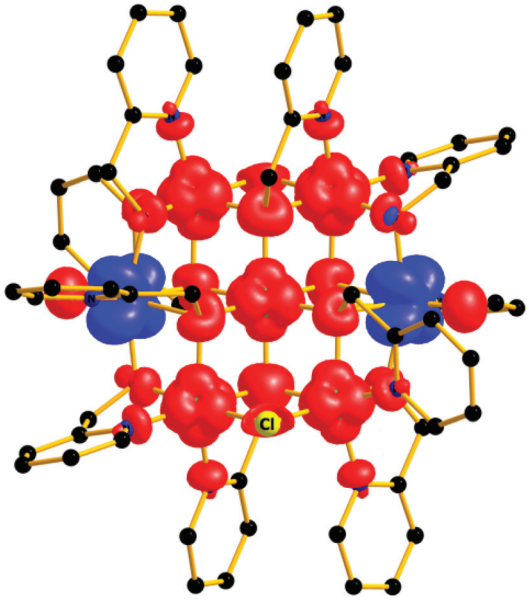

Fig. 5 Spin density plot of the ground state of complex **1** at an isosurface value of 0.0065 e $bohr^{-3}$.

Table 2 Comparison of the best-fit and theoretical J values of complexes **1** and **2**

Complex	Method	J_1/ cm^{-1}	J_2/ cm^{-1}	J_3/ cm^{-1}	J_4/ cm^{-1}
1	Fit	1.30	−3.49	1.30	−3.49
1	DFT	0.11	−9.89	3.18	0.23
2	Fit	−0.45	−4.85	−0.45	−4.85
2	NEVPT2-QDPT-EHA + fit	−1.48	−8.19	3.72	6.13

For **2** the magnetic anisotropy parameters of the Co(II) centres were estimated by *ab initio* calculations. In this case the zfs parameters (D_{Co}) were found to be much larger than the exchange parameters as Co(II) ions in distorted octahedral environments possess sizeable magnetic anisotropy.[27–31] The local anisotropy parameters, computed from the NEVPT2-QDPT-EHA level of theory, were found to be $D_{Co(ring)} = \pm 87\ cm^{-1}$, $E/D = 0.27$ and $D_{Co(central)} = +82\ cm^{-1}$, $E/D = 0.19$ (Tables S5 and S6†), about a factor of four larger than the best fit D_{Co} parameter obtained by numerically fitting the experimental data to spin-Hamiltonian (1). Due to the very strong anisotropy, single determinant DFT calculations are unable to yield reasonable exchange values ($J_1 = -18.7\ cm^{-1}$, $J_2 = 54.42\ cm^{-1}$, $J_3 = -0.66\ cm^{-1}$ and $J_4 = 84.71\ cm^{-1}$). Thus, attempts to simulate the experimental susceptibility and magnetisation data of **2** using the DFT computed J values along with the highly anisotropic D values were unsuccessful. Therefore, for the quantitative interpretation of the experimental data, we fix the anisotropy parameters of the Co(II) centres to those calculated as described above and fit the four exchange parameters in spin-Hamiltonian (1). This resulted in the best fit parameters: $J_1 = -1.48\ cm^{-1}$, $J_2 = -8.19\ cm^{-1}$, $J_3 = 3.72\ cm^{-1}$ and $J_4 = 6.13\ cm^{-1}$ (solid blue line and dashed lines in Fig. 3).

In order to further investigate the origin of the magnetic anisotropy of the Co^{II} ions, we have plotted the ligand-field d-orbital splitting diagram of the central Co ion (M2 in Fig. 1) of complex **2** (Fig. 6). 58% of the ground state electronic con-

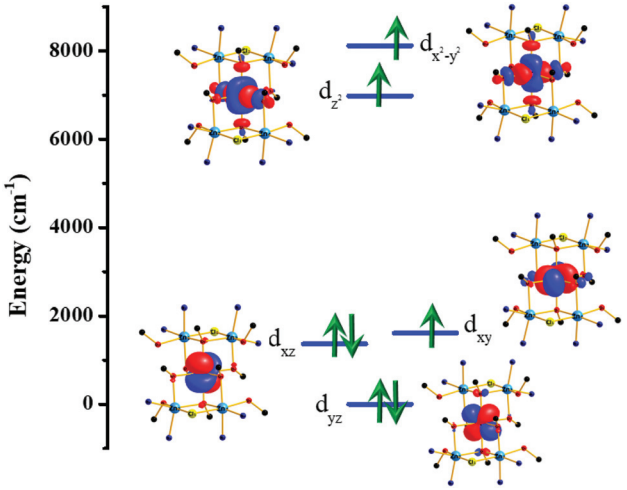

Fig. 6 *Ab initio* ligand field d-orbital splitting diagram of the central Co^{II} ion.

figuration consists of $(d_{yz})^2(d_{xz})^2(d_{xy})^1(d_{z^2})^1(d_{x^2-y^2})^1$. The major contribution towards the very large D value arises from the first two excited states (Table S5†) which lie 619 cm^{-1} and 1294 cm^{-1} above the ground state and contribute 38 cm^{-1} and 24 cm^{-1}, respectively, towards the overall D value. These two excited states arise from the $d_{xz}/d_{yz} \rightarrow d_{xy}$ spin allowed electronic transitions. The multi-determinant nature of the wavefunction also suggests that a single electronic configuration is not sufficient to describe the true electronic structure of the Co^{II} centres. The anisotropy axes (D_{zz} axes) of the five Co^{II} ions are oriented in a 'random' fashion (Fig. S9†).

Conclusions

A structurally unique Anderson-type wheel of formula $[(VO)_2M_5(hmp)_{10}Cl_2](ClO_4)_2{\cdot}2MeOH$ (M = Ni, Co), in which the V^{IV} ions oppose each other in the outer wheel has been synthesised *via* solvothermal methods using the pro-ligand hmpH. Complexes **1–2** are rare examples of heterometallic V^{IV}–Ni^{II}/Co^{II} cluster compounds. Magnetic susceptibility and magnetisation studies reveal competing ferro- and antiferromagnetic exchange interactions; the strongest interaction in each case being the antiferromagnetic exchange between $M^{II}_{(ring)}$–(O)(O)–$V^{IV}_{(ring)}$ – consistent between experiment and theory. The observation of structurally analogous homo- and heterometallic, and homo- and heterovalent $[M_7]$ Anderson wheels containing d- (and s-) block metals in the II+, III+ and IV+ oxidation states points toward the exceptional stability of the structure type. It further suggests that an enormous number of similar $[M_7]$ complexes containing a combination of different metal ions in different oxidation states and displaying different magnetic behaviours have yet to be isolated. Given the prevalence of "brucite-like" molecular 2D sheets based on shared $[M_3]$ triangular building blocks in 3d polymetallic coordination chemistry,[11] we also speculate that similar species to **1** and **2** but with larger nuclearities in sheet-like "2D" frameworks can be formed.

Conflicts of interest

There are no conflicts to declare.

Acknowledgements

We thank the EPSRC for funding grants EP/P025986/1 and EP/N01331X/1. EKB, GR and AS thank the British Council, UKIERI grant 2017-18-04. S. P. thanks the VILLUM FONDEN for research grant 13376. AS thanks IIT Bombay for funding. GR would like to thank DST and SERB (CRG/2018/000430; DST/SJF/CSA-03/2018-10; SB/SJF/2019-20/12), UGC-UKIERI (184-1/2018(IC)) and SUPRA (SPR/2019/001145) for funding.

Notes and references

1 M. T. Pope and A. Müller, *Angew. Chem., Int. Ed. Engl.*, 1991, **30**, 34.
2 O. Kahn, J. Galy, Y. Journaux, J. Jaud and I. Morgenstern-Badarau, *J. Am. Chem. Soc.*, 1982, **104**, 2165.
3 S. Ferlay, T. Mallah, R. Ouahès, P. Veillet and M. Verdaguer, *Nature*, 1995, **378**, 701.
4 S. L. Castro, Z. M. Sun, C. M. Grant, J. C. Bollinger, D. N. Hendrickson and G. Christou, *J. Am. Chem. Soc.*, 1998, **120**, 2365.
5 See for example: (*a*) J. Schnack, M. Luban and R. Modler, *Europhys. Lett.*, 2001, **56**, 863; (*b*) G. Chaboussant, S. T. Ochsenbein, A. Sieber, H.-U. Güdel, H. Mutka, A. Müller and B. Barbara, *Europhys. Lett.*, 2004, **66**, 423; (*c*) V. V. Maslyuk, I. Mertig, O. V. Farberovich, A. Tarantul and B. Tsukerblat, *Eur. J. Inorg. Chem.*, 2013, 1897.
6 (*a*) J. M. Zadrozny, J. Niklas, O. G. Poluektov and D. E. Freedman, *J. Am. Chem. Soc.*, 2014, **136**, 15841; (*b*) M. Atzori, L. Tesi, E. Morra, M. Chiesa, L. Sorace and R. Sessoli, *J. Am. Chem. Soc.*, 2016, **138**, 2154.
7 See for example: (*a*) R. H. Laye, F. K. Larsen, J. Overgaard, C. A. Muryn, E. J. L. McInnes, E. Rentschler, V. Sanchez, S. J. Teat, H. U. Güdel, O. Waldmann, G. A. Timco and R. E. P. Winpenny, *Chem. Commun.*, 2005, 1125; (*b*) T. Kurata, A. Uehara, Y. Hayashi and K. Isobe, *Inorg. Chem.*, 2005, **44**, 2524.
8 See for example: (*a*) E. Antonova, C. Näther, P. Kögerler and W. Bensch, *Inorg. Chem.*, 2012, **51**, 2311; (*b*) M. Rasmussen, C. Näther, J. van Leusen, P. Kögerler, L. Zhechkov, T. Heine and W. Bensch, *Inorg. Chem.*, 2017, **56**, 7120; (*c*) F. Lia, L. Xua, Y. Weib, X. Wanga, W. Wanga and E. Wang, *J. Mol. Struct.*, 2005, **753**, 61; (*d*) Z. Shi, J. Peng, C. J. Gómez-García, S. Benmansour and X. Gua, *J. Solid State Chem.*, 2006, **179**, 253.
9 (*a*) K. K. Nanda, S. Mohanta, S. Ghosh, M. Mukherjee, M. Helliwell and K. Nag, *Inorg. Chem.*, 1995, **34**, 2861;

(*b*) S.-Z. Du, J. Feng, L. An and X.-M. Lu, *Z. Anorg. Allg. Chem.*, 2012, **638**, 411; (*c*) M. D. Glick, R. L. Lintvedt, D. P. Gavel and B. Tomlonovic, *Inorg. Chem.*, 1976, **15**, 1654; (*d*) D. Mandal, P. B. Chatterjee, R. Ganguly, E. R. T. Tienik, R. Clérac and M. Chaudhury, *Inorg. Chem.*, 2008, **47**, 584; (*e*) B.-S. Kang, X.-J. Wang, C.-Y. Su and H.-Q. Liu, *Transition Met. Chem.*, 1999, **24**, 712.

10 M. I. Khan, S. Tabussum, R. J. Doedens, V. O. Golub and C. J. O'Connor, *Inorg. Chem.*, 2004, **43**, 5850.

11 (*a*) H. W. L. Fraser, G. S. Nichol, D. Uhrín, U. G. Nielsen, M. Evangelisti, J. Schnack and E. K. Brechin, *Dalton Trans.*, 2018, **47**, 11834; (*b*) H. W. L. Fraser, G. S. Nichol and E. K. Brechin, *Dalton Trans.*, 2018, **47**, 15530.

12 G. M. Sheldrick, *Acta Crystallogr., Sect. C: Cryst. Struct. Commun.*, 2015, **71**, 3.

13 O. V. Dolomanov, L. J. Bourhis, R. J. Gildea, J. A. K. Howard and H. Puschmann, *J. Appl. Crystallogr.*, 2009, **42**, 339.

14 M. J. Frisch, G. W. Trucks, H. B. Schlegel, G. E. Scuseria, M. A. Robb, J. R. Cheeseman, G. Scalmani, V. Barone, B. Mennucci, G. A. Petersson, H. Nakatsuji, M. Caricato, X. Li, H. P. Hratchian, A. F. Izmaylov, J. Bloino, G. Zheng, J. L. Sonnenberg, M. Hada, M. Ehara, K. Toyota, R. Fukuda, J. Hasegawa, M. Ishida, T. Nakajima, Y. Honda, O. Kitao, H. Nakai, T. Vreven, J. A. Montgomery Jr., J. E. Peralta, F. Ogliaro, M. Bearpark, J. J. Heyd, E. Brothers, K. N. Kudin, V. N. Staroverov, T. Keith, R. Kobayashi, J. Normand, K. Raghavachari, A. Rendell, J. C. Burant, S. S. Iyengar, J. Tomasi, M. Cossi, N. Rega, J. M. Millam, M. Klene, J. E. Knox, J. B. Cross, V. Bakken, C. Adamo, J. Jaramillo, R. Gomperts, R. E. Stratmann, O. Yazyev, A. J. Austin, R. Cammi, C. Pomelli, J. W. Ochterski, R. L. Martin, K. Morokuma, V. G. Zakrzewski, G. A. Voth, P. Salvador, J. J. Dannenberg, S. Dapprich, A. D. Daniels, O. Farkas, J. B. Foresman, J. V. Ortiz, J. Cioslowski and D. J. Fox, *Gaussian 09, Revision D.01*, Gaussian, Inc., Wallingford CT, 2013.

15 F. Neese, *Wiley Interdiscip. Rev.: Comput. Mol. Sci.*, 2018, **8**, e1327.

16 R. Maurice, R. Bastardis, C. de Graaf, N. Suaud, T. Mallah and N. Guihéry, *J. Chem. Theory Comput.*, 2009, **5**, 2977.

17 F. E. Kakaroni, A. Collet, E. Sakellari, D. I. Tzimopoulos, M. Siczek, T. Lis, M. Murrie and C. J. Milios, *Dalton Trans.*, 2018, **47**, 58.

18 O. Cador, D. Gatteschi, R. Sessoli, F. K. Larsen, J. Overgaard, A.-L. Barra, S. J. Teat, G. A. Timco and R. E. P. Winpenny, *Angew. Chem., Int. Ed.*, 2004, **43**, 5196.

19 H. Press, S. A. Teukolsky, W. T. Vetterling and B. P. Flannery, *Numerical Recipes in C: The Art of Scientific Computing*, Cambridge University Press, Cambridge, 2nd edn, 1992.

20 L. N. Zheng, S. Y. Zhang, K. Li, W. Q. Chen, Y. M. Chen, B. Xu, B. Hu, Y. H. Li and W. Li, *J. Mol. Struct.*, 2010, **984**, 153.

21 M. K. Hänninen, J. Välivaara, J. Cano, R. Sillanpää and E. Colacio, *Eur. J. Inorg. Chem.*, 2016, 1192.

22 S. S. Massoud, M. Spell, C. C. Ledet, T. Junk, R. Herchel, R. C. Fischer, Z. Trávníček and F. A. Mautner, *Dalton Trans.*, 2015, **44**, 2110.

23 L. Noodleman, *J. Chem. Phys.*, 1981, **74**, 5737.

24 G. Rajaraman, K. E. Christensen, F. K. Larsen, G. A. Timco and R. E. P. Winpenny, *Chem. Commun.*, 2005, 3053.

25 M. A. Halcrow, J.-S. Sun, J. C. Huffman and G. Christou, *Inorg. Chem.*, 1995, **34**, 4167.

26 R. Sen, A. M. L. Lopes, Z. Lin, P. Brandão and J. P. Araújo, *Eur. J. Inorg. Chem.*, 2019, 3840.

27 F. El-Khatib, B. Cahier, F. Shao, M. López-Jordà, R. Guillot, E. Rivière, H. Hafez, Z. Saad, J. J. Girerd, N. Guihéry and T. Mallah, *Inorg. Chem.*, 2017, **56**, 4601–4608.

28 S. Gómez-Coca, A. Urtizberea, E. Cremades, P. J. Alonso, A. Camón, E. Ruiz and F. Luis, *Nat. Commun.*, 2014, **5**, 4300.

29 F. Shao, B. Cahier, E. Rivière, R. Guillot, N. Guihéry, V. E. Campbell and T. Mallah, *Inorg. Chem.*, 2017, **56**, 1104.

30 J. Vallejo, I. Castro, R. Ruiz-García, J. Cano, M. Julve, F. Lloret, G. De Munno, W. Wernsdorfer and E. Pardo, *J. Am. Chem. Soc.*, 2012, **134**, 15704.

31 V. V. Novikov, A. A. Pavlov, Y. V. Nelyubina, M.-E. Boulon, O. A. Varzatskii, Y. Z. Voloshin and R. E. P. Winpenny, *J. Am. Chem. Soc.*, 2015, **137**, 9792.